Large-Scale Effects on Local Small-Scale Chaotic Solutions to Burgers' Equation

J.M. McDonough* and R.J. Bywater†
The Aerospace Corporation, El Segundo, California

The effects of local variations in velocity and a pressure-gradient-like forcing term are studied in detail for the small-scale equations of an additive decomposition of Burgers' equation. Computations are presented for relatively high Reynolds numbers, $O(10^5)$, for which it is shown that transitions to chaos (turbulence) can occur with respect to each of the velocity and pressure gradients. The influence of overall Reynolds number and the local large-scale velocity are also considered in less detail. Flow regime maps summarizing the effects of velocity and pressure gradients, and Reynolds number, are displayed. Numerical criteria are presented for consistently employing the Burgers' equation strange attractor as a small-scale (subgrid) turbulence model.

Introduction

IT has been accepted for some time that the Navier-Stokes equations should be capable of simulating turbulent fluid behavior without use of the various averaging procedures that require closure models. In a sense, this was suggested in the work of Ruelle and Takens,[1] which also indicated that the nature of turbulence is probably distinctly different from that embodied in the Landau-Hopf[2] viewpoint. In particular, it is proven in Ref. 1 that equations of the form of the Navier-Stokes equations can exhibit the temporally chaotic solutions of a strange attractor after only a few bifurcations (flow transitions) and that these solutions are "generic," i.e., likely to occur. It is important to note that this description of the onset of turbulence is supported by numerous laboratory experiments (e.g., Gollub and Benson[3]), although it is becoming apparent that somewhat more complicated bifurcation sequences than those predicted in Ref. 1 may occur. In particular, intermittency of the form studied by Pomeau and Manneville (see Ref. 4) and the period-doubling (subharmonic) bifurcations of Feigenbaum[5] are typically found. These may occur as separate routes to turbulence, or they may be found embedded in a Ruelle-Takens sequence of bifurcations.

Despite the fact that the Navier-Stokes equations produce turbulent solutions at sufficiently high Reynolds number *Re*, in practice it has been impossible to resolve the extremely small length and time scales associated with typical high *Re* turbulent flows. Recognition of this fact motivated the development of large eddy simulation (LES). In this technique, the large-scale motion typically observed in turbulent flows, i.e., the coherent structures,[6] is computed "exactly," using high-accuracy standard numerical methods applied to filtered versions of the Navier-Stokes equations. The effects of small-scale turbulent motion are modeled via subgrid scale models and are included in the overall computations through terms similar to Reynolds stress terms arising from the large-scale filtering procedure (c.f. Rogallo and Moin[7] for a current review of LES).

Although LES has successfully modeled certain flows, it has not produced results at high *Re*, where one really expects to find turbulent behavior. Moreover, the basic use of averaging and/or filtering procedures in general has been questioned by Deissler,[8] and "direct" simulations are now being conducted by several investigators (e.g., Grötzbach[9] and Feiereisen et al.[10]). Nevertheless, these direct simulations are limited to low values of *Re* due to limitations of current computing hardware. This state of affairs has motivated introduction of an unfiltered decomposition procedure,[11,12] which is similar to LES in some respects but very different in other ways. In particular, the present method decomposes the problem into large-scale (coherent) and small-scale (turbulent) parts without formal filtering. Hence, the small scale is directly computed, rather than modeled as an additional forcing term of the large-scale equations. Furthermore, the small-scale solutions are obtained locally (see below) from systems of equations similar to the original governing equations of the problem. This local formalism permits a high degree of spatial and temporal resolution not presently attainable in direct simulations, and it results in the chaotic solutions of a strange attractor for sufficiently high *Re*.

In Refs. 11 and 12, small-scale solutions were obtained for a few specific large-scale solutions. In the present study, we systematically investigate the effects on the small-scale solutions by varying three of the main large-scale solution properties, namely, the value of the last Fourier coefficient supported by the calculation, and the local values of the large-scale velocity gradient and pressure gradient. As in Refs. 11 and 12, the present research employs Burgers' equation rather than the full Navier-Stokes equations. Nevertheless, for reasons given below (and from previous studies[11-13]), we believe that the results presented here will apply to the Navier-Stokes equations, at least in a general way, and provide a format for fully three-dimensional Navier-Stokes computations.

Analysis

The large-scale/small-scale decomposition employed to obtain the equations of this study has been treated in detail.[11,12] We summarize the main steps for completeness in the present work.

The form of Burgers' equation considered here is

$$U_t + \frac{1}{2}(U^2)_x - \frac{1}{Re}U_{xx} = -P_x \tag{1}$$

This equation embodies all the main mathematical features of the Navier-Stokes equations when $P_x \not\equiv 0$. This nonhomogeneous function, which must be assigned, plays the role of a pressure gradient. Just as the pressure field strongly influences the flowfield of a Navier-Stokes solution, the nonhomogeneous function is of major importance in setting

Received July 2, 1985; presented as Paper 85-1653 at the AIAA 18th Fluid Dynamics and Plasmadynamics and Lasers Conference, Cincinnati, OH, July 16-18, 1985; revision received March 25, 1986.

*Member of Technical Staff, Fluid Mechanics Department.
†Engineering Specialist, Fluid Mechanics Department. Member AIAA.

the form of solutions to Eq. (1). In Ref. 13, P_x is varied randomly in time; when it is in a certain amplitude range, solutions to Eq. (1) exhibit the $-5/3$ Kolmogorov inertial range exponent. Reference 11 shows that varying the small-scale part of P_x yields a bifurcation sequence similar to that of the Ruelle-Takens theory for the Navier-Stokes equations as Re is varied.

As in Refs. 11 and 12, we employ the additive decomposition

$$U=u+u^*, \qquad P=p+p^* \tag{2}$$

where the asterisk (*) denotes the small-scale part. After substituting Eq. (2) into Eq. (1), we obtain the large-scale and small-scale equations (without averaging or filtering) with the introduction of the decomposition parameter β. The resulting large-scale equation is

$$u_t+\frac{1}{2}(u^2)_x+(1-\beta)(u^*u)_x-\frac{1}{Re}u_{xx}=-p_x$$

and the small-scale equation to be studied herein is

$$u_t^*+\frac{1}{2}(u^{*2})_x+\beta(uu^*)_x-\frac{1}{Re}u_{xx}^*=-p_x^* \tag{3}$$

Note, as shown in Ref. 14, p. 517, that this additive decomposition would be trivially valid were it not for the nonlinear term in Eq. (1). We have handled this term in the following way:

$$\frac{1}{2}(u^2)_x=\frac{1}{2}[(u+u^*)^2]_x=uu_x+u^*u_x+uu_x^*+u^*u_x^*$$

The second and third terms combine as $(uu^*)_x$, which we express as

$$(uu^*)_x=\beta(uu^*)_x+(1-\beta)(uu^*)_x$$

for any value of β.

The parameter β controls the large-scale/small-scale interaction. For example, in the limit $\beta=1$, the effect of large-scale advection is transferred to the small scale, but not vice versa, consistent with the belief that in most turbulent flows this unidirectional transfer is dominant; $\beta=1$ has been used in the present study. In future work, the role of β (not necessarily equal to unity) in consistently coupling the large and small scales will be explored. In particular, it is reasonable to expect that β need not have the same value at every finite difference grid point of the large-scale computation, and this fact emphasizes the need to predict β theoretically. It has been shown by Yakhot and Orszag[15] that renormalization group techniques can be used to calculate an analogous parameter arising in their analysis of large eddy simulation. We are adapting this method to predict β in the complete large-scale/small-scale decomposition of Burgers' equation.

Equation (3) is solved by means of a local Galerkin approximation at each grid point of the large-scale discretization. At the ith such point (see Fig. 1), we have

$$u_i^*(x,t)=\sum_{k=1}^{K}a_k(t)\sin\ \alpha_k\left(\frac{x-\bar{x}_i}{h}\right),$$

$$x\in\left[x_i-\frac{h}{2},x_i+\frac{h}{2}\right] \tag{4}$$

where h is the spatial discretization step size of the large-scale calculation, $\alpha_k\equiv k\pi$, and $\bar{x}_i=x_i-h/2$. Substitution of Eq. (4) into Eq. (3) and application of the usual Galerkin procedure leads to the following system of ordinary differential equations:

$$\dot{a}_1=0 \tag{5a}$$

and

$$\dot{a}_k=-\frac{C\pi}{2h}\sum_{\ell,m=1}^{K}(\ell A_{k\ell m}+mA_{km\ell})a_\ell a_m$$

$$-\left[\beta u_x+\frac{1}{Re}\left(\frac{k\pi}{h}\right)^2\right]a_k-\hat{p}_{x,k}^*\quad k=2,3,\ldots,K. \tag{5b}$$

In Eq. (5b), C is the normalization constant and the $A_{k\ell m}$ are the usual Galerkin triple products arising from the advective term in Eq. (3). Also, $\hat{p}_{x,k}^*$, is formally the kth Fourier coefficient of p_x^*. In the present study, since p_x^* is itself an assigned (local) constant, we have somewhat arbitrarily defined

$$\hat{p}_{x,k}^*\equiv\frac{p_x^*}{2k}[1+(-1)^k]$$

Other definitions have been used (see Refs. 11 and 12). Specific quantitative details of solutions are different for different definitions of $\hat{p}_{x,k}^*$, but the observed bifurcation sequences occur for various $\hat{p}_{x,k}^*$ representations.

It is of interest to consider some details regarding Eq. (5). We first note that from Eq. (5a) $a_1\equiv$ const. In fact, this constant is related to the local value of the large-scale velocity and scales with the highest Fourier mode supported by the large-scale discretization. This value will be systematically varied in the present study to assess the effects of the local large-scale velocity on the small-scale solution. By fixing a_1, we consistently couple the large- and small-scale contributions and in this way provide energy to drive the small scale. Note that this requirement has been recognized in previous investigations, e.g., Qian,[13] but has always been handled in an ad hoc manner.

We next consider the length scale h of the Galerkin representation. We observe that h should be viewed as a scaling of the wave numbers. As such, it is clear that decreasing h results in a corresponding increase in the effective value of K. It is this scaling property, in conjunction with use of the local approximation, that leads to the high spatial resolution of the method, as indicated in Fig. 1. From this figure, note that a single mode on the subinterval of length h provides local resolution equivalent to L/h modes on the interval of length L.

The next term in Eq. (5) to be discussed is u_x. This local large-scale velocity gradient is (proportional to) a local flow acceleration. It is interesting to observe that this term (when $\beta>0$) provides an additive contribution to the dissipation term in the Galerkin representation, Eq. (5a). In fact, if $u_x>0$, dissipation is increased while $u_x<0$ implies a decrease in dissipation.

The Re term in Eq. (5) contains the large-scale Re. However, this must be rescaled in the present local context. It is to be expected that the high spatial resolution afforded by the decomposition and local formalism applied in the present work requires high temporal resolution for the high-frequency content of the small-scale component. This is manifest in the Re term of Eq. (5). The large-scale, overall Reynolds number appearing in that term of the small-scale equation leads to the commonly encountered need to rescale in high Re flows. Simply rescaling by h does not scale the time or Reynolds number appropriately. It is necessary to scale with the Reynolds number based on an appropriate small-scale velocity/length scale combination to effect a stretching of the local time scale resulting in the required improvement in temporal resolution. In practice, smaller time steps are used for the small-scale component equation to accomplish this.

Numerical Analysis

It is important to observe, as noted by Huang and McDonough,[16] that problems associated with a strange attractor are not well posed with respect to a uniform norm, due to sensitive dependence on initial conditions. Conse-

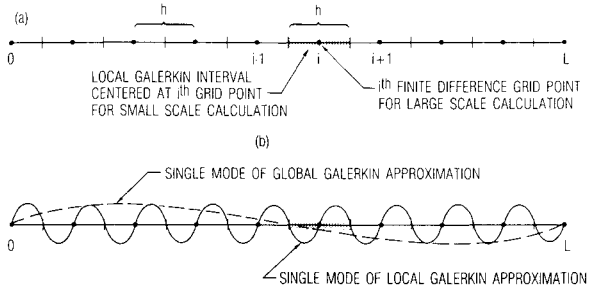

Fig. 1 Finite difference–local Galerkin representation: a) finite difference grid showing local Galerkin interval; b) comparison of global vs local Galerkin resolution.

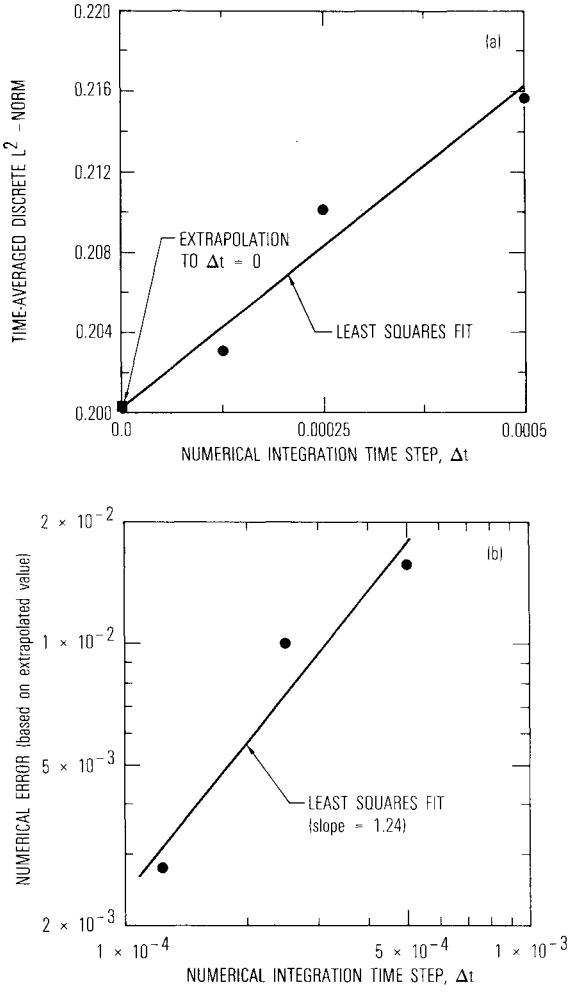

Fig. 2 Time-averaged, least squares L^2 convergence of grid function approximations to chaotic solutions ($p_x^* = -42.5$, $u_x = 1$, $Re = 10^5$, $a_1 = 0.075$).

quently, usual methods of verifying the numerical analytic procedures are of little use, since convergence occurs only in the sense of global properties of the solution (e.g., the time-averaged L^2 norm).

Computed results were obtained using a second-order explicit Runge-Kutta method (Heun's method[17]) with constant time step $\Delta t = 0.00025$ (except as indicated below); integrations were continued for 8192 time steps. This value of Δt was less than half that required to maintain stability (as governed by the viscous stability limit). Runs for certain of the chaotic cases were repeated with $2\Delta t$ and $(1/2)\Delta t$. Such global properties as frequency of velocity direction reversal, time-averaged L^2 norm, and average velocity variation per time step were found to change by less than 5% in going from $2\Delta t$ to Δt, and then from Δt to $(1/2)\Delta t$. Figure 2 demonstrates this phenomenon for the time-averaged L^2 norm (the average energy of the flow), as well as showing that the numerical computations do, in fact, converge. Figure 2a shows that as Δt is decreased, the time-averaged L^2 norm

$$\frac{1}{T}\left[\int_0^T u^2(t)\mathrm{d}t\right]^{1/2}$$

converges in the least-squares sense to a value slightly larger than 0.2. This value is used as the "exact" value for computing the numerical errors (shown in Fig. 2b) for each finite Δt of the convergence tests in a manner analogous to employing a Richardson extrapolation for verification of pointwise convergence. It is observed that convergence occurs as $(\Delta t)^{1.24}$ for the present set of data.

In addition to purely numerical analytic difficulties with strange attractors, there is also the problem of function analytical representation. As evidenced in the work of Franceschini,[18] grossly truncated Galerkin representations of chaotic solutions are not convergent in the usual sense of L^2. Moreover, Treve[19] has shown that, without modification, truncated Galerkin approximations to the Navier-Stokes equations are not energy-conserving. However, in Ref. 20 it was demonstrated that the local Galerkin representation, as presented herein, of Burgers' equation converges in the least-squares sense in the time-averaged L^2 norm. We have employed this information in the present study to set the values of h and K so as to obtain consistent models of spectral energy transfer from the large scale, through the inertial range, and on into the dissipation range.

Our procedure is based on two main criteria. First, the Fourier representations [Eq. (4)] are required to be "converged" in the sense that at any time the limit of the (C,1)-Césaro absolute mean

$$\lim_{k\to\infty} \sigma_k = \sigma, \qquad \sigma_k = \frac{1}{k}\sum_{j=1}^{k} |a_j|$$

is reasonably well converged. This is demonstrated in Fig. 3a for a specific case. These results show that for this 10-mode representation, the Césaro partial sums have reached a nearly constant value starting with the sixth partial sum. It is also shown in Ref. 20 that as the number of modes used in the Galerkin representation is increased above 10, the Césaro sums continue to converge to the same value. This weak form of convergence is sensitive mainly to the value of Re and not to the other parameters, such as u_x and p_x^*. As indicated in Fig. 3a for a chaotic solution, nine Fourier modes (10 modes, if $a_1 = \text{const}$ is counted) are sufficient to achieve a fair degree of convergence (in the above sense) at $Re = 10^5$. Results in Ref. 20 indicate that the required number of modes is an increasing function of Re, in basic agreement with Constantin et al.[21]

The second criterion to be satisfied is that the time-averaged, squared Fourier coefficients corresponding to chaotic solutions have a least-squares decay rate slightly larger in magnitude than the Kolmogorov $-5/3$ inertial range exponent. When this holds, energy may be transferred from the large scale, through the inertial range, and on into the dissipation range. This criterion is used to establish the value of the large-scale finite difference grid spacing h. It was found that $h = 0.009$ led to satisfaction of this condition with $Re = 10^5$ and $K = 10$, as indicated in Fig. 3b for a specific case. (It is worth mention that this combination of h and K corresponds to 1111 modes in a global Galerkin approximation on [0,1], with a corresponding cell-Re approximately between unity and 20.) As seen from this figure, when the criterion is satisfied, the energy spectrum exhibits three distinct wave-number regions corresponding to 1)

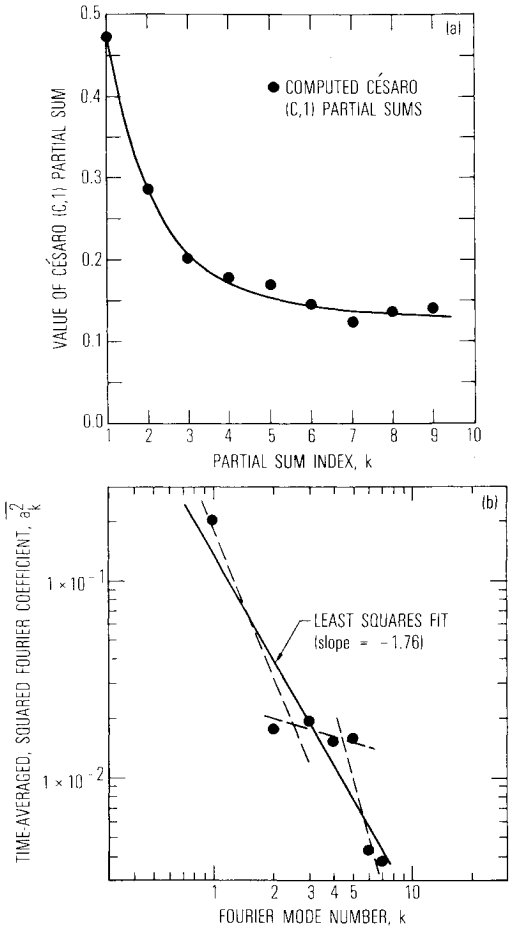

Fig. 3 Césaro summability and L^2 convergence of time-averaged Fourier coefficients of chaotic solutions ($p_x^* = -30$, $u_x = -7$, $Re = 10^5$, $a_1 = 0.075$).

large-scale phenomena, 2) an intermediate range, and 3) dissipation range. The required value of h is not sensitive to changes in u_x and p_x^*.

Results and Discussion

We now present detailed discussions of the effects of varying u_x, p_x^*, Re, and a_1. All results were obtained using the initial conditions

$$a(0) = (a_1, 0.25, 0.125, 0.0625, 0.04, 0.028,$$
$$0.02, 0.015, 0.012, 0.01)^T$$

where $a_1 = 0.075$ unless specifically noted to the contrary. No investigation has been made regarding the extent of the basins of attraction that include this initial condition.

Figure 4 summarizes results for variation of u_x in the range $-3.0 \le u_x \le 30.0$ with $p_x^* = -50$ and $Re = 10^5$. In Fig. 4a, we depict the velocity time series for a slightly decelerated flow which, after a short (but fairly violent) initial transient, becomes steady. Figure 4b represents the zero-acceleration situation $u_x = 0$. The general behavior of growing oscillations followed by intermittent high-amplitude turbulent bursts is characteristic of the Pomeau-Manneville[4] route to turbulence. It is first seen for u_x between -2 and -1.5, with the bifurcation occurring directly from the steady solution. It is interesting to note that this behavior is also observed in solutions of the Lorenz equations[22]; moreover, it has been seen in laboratory experiments involving a toroidal thermosyphon.[23]

Figure 4c displays a fully turbulent flow corresponding to $u_x = 4$. This flow consists of fairly low-frequency, high-amplitude oscillations, which are nonperiodic and therefore chaotic. Short bursts of very high-frequency behavior are distributed throughout in a nonperiodic fashion. This chaotic behavior associated with a strange attractor exists for $0 < u_x < 8$. For $u_x = 8$, we show in Fig. 4d the beginning of a sequence of subharmonic, or period-doubling, bifurcations (see Ref. 5), which results in the chaotic behavior observed for $u_x = 4$ as u_x is reduced. The remnants of the subharmonic velocity trace of Fig. 4d can be seen at various intervals in Fig. 4c. Figure 4e depicts a periodic flow at $u_x = 20$ prior to the onset of the period-doubling bifurcations. The periodic flow regime is encountered for u_x in the range $10 < u_x < 25$. Between $u_x = 25$ and $u_x = 30$, a Hopf bifurcation from steady flow, shown in Fig. 4f, occurs.

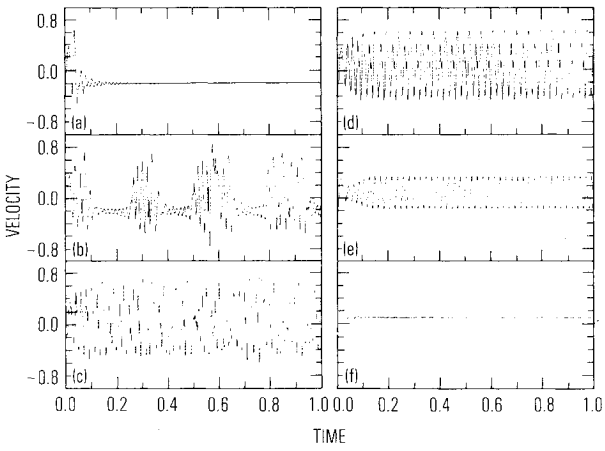

Fig. 4 Velocity time series for various values of velocity gradient, u_x: a) −3.0, b) 0.0, c) 4.0, d) 8.0, e) 20.0, f) 30.0.

It is worth noting that large positive values of u_x correspond to an accelerating flowfield; in the presence of a favorable pressure gradient, we would expect this to be stable. As u_x is decreased and p_x^* held fixed, we expect that stability will be lost; this is first seen in our calculations in a bifurcation to periodic flow. Further decreases in u_x lead ultimately to the onset of subharmonic bifurcations and finally to turbulence. This sequence of transitions is basically a Ruelle-Takens [1] sequence, but with an embedded Feigenbaum period-doubling transition replacing the quasiperiodic flow regime. Then, as the flow is locally decelerated (still in the presence of a favorable pressure gradient), turbulent behavior becomes intermittent and ultimately ceases. From the mathematical standpoint, it is clear from Eq. (5b) that the dissipation is being reduced; dissipation is necessary for the existence of a strange attractor. Thus, return to steady flow is not altogether surprising.

As u_x is decreased even further, the nature of the mathematical solution changes; due to high-frequency components, the 10 mode representations used here are not adequate. We shall not specifically treat these results, but we mention that ultimately the 10 mode solutions undergo a Ruelle-Takens sequence of bifurcations back to turbulence: steady, periodic, quasiperiodic, chaotic, as u_x is decreased to a value of -25.

The effects of pressure gradient p_x^* on the solutions to the local Burgers' equation have been treated in some detail in Refs. 11 and 12 for $u_x = 0$, $a_1 = 0.025$. We shall expand on these results in this study. In Fig. 5, we present power spectral densities (PSDs) of velocity time series computed with $u_x = 5$, $a_1 = 0.075$, $Re = 10^5$, and various values of p_x^*. These PSDs were constructed from the last 4096 data points of the computation, with the mean subtracted, and the resulting data processed with a GEO window,[24] as in our previous studies.[11,12] The frequencies have been normalized to the Nyquist frequency.

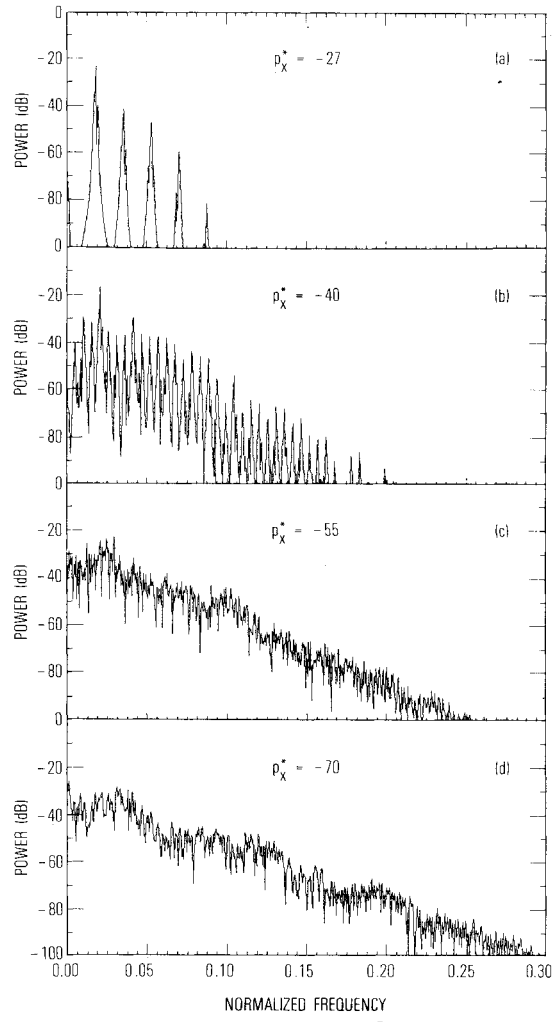

Fig. 5 Power spectral densities for $Re = 10^5$, $u_x = 5$, $a_1 = 0.075$: a) periodic, $p_x^* = -27$; b) subharmonic, $p_x^* = -40$; c) turbulent, $p_x^* = -55$; d) intermittent, $p_x^* = -70$.

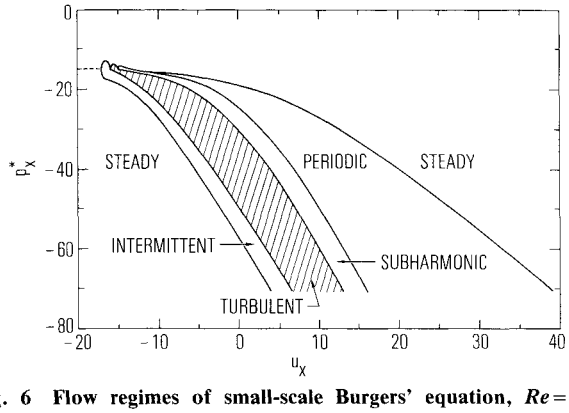

Fig. 6 Flow regimes of small-scale Burgers' equation, $Re = 10^5$, $a_1 = 0.075$.

Figure 5a presents results for $p_x^* = -27$, for which the flow is periodic with a (normalized) fundamental frequency of $\simeq 0.018$. This particular value of p_x^* is near the center of the region of periodic flow (see Fig. 6.) In Figure 5b we display an interesting subharmonic case for $p_x^* = -40$. The PSD gives the appearance of a phase lock at higher frequencies, but it is clear from the lower frequencies that two period doublings have occurred and that a third is imminent. In particular, the reason for the phase-locked appearance is that the halved frequencies have grown to an amplitude nearly equal to that of the various harmonics of the fundamental.

Table 1 Flow type and Fourier decay exponent vs p_x^*

p_x^*	Flow type	Time-averaged Fourier decay exponent, q	Least-squares correlation coefficient
−10	Steady	−1.96	0.97
−20	Periodic	−2.41	0.74
−30	Subharmonic	−1.91	0.83
−50	Turbulent	−1.73	0.95

Table 2 Effects of a_1 ($p_x^* = -42.5$, $u_x = 1$, $Re = 10^5$)

a_1	Flow type
−0.125	Steady
−0.100	Turbulent
−0.075	Turbulent
−0.050	Turbulent
−0.025	Turbulent
0.0	Periodic
0.025	Intermittent
0.050	Intermittent
0.075	Turbulent
0.100	Turbulent
0.125	Steady

This behavior is quite analogous to that reported in Ref. 3 for laboratory experiments in Bénard convection. Figure 5c presents a turbulent case with $p_x^* = -55$. This PSD is basically broadband noise with power no longer concentrated at distinct frequencies. The intermittent case $p_x^* = -70$, shown in Fig. 5d, is similar but with power distributed over an even wider frequency range. It is, in fact, not possible to detect intermittency from this figure, but the phenomenon was clearly indicated from the time series (not shown, but similar to Fig. 4b).

Overall, the effect of increasing the magnitude of p_x^*, with all other parameters fixed, is to traverse a sequence of bifurcations from steady flow to periodic, then to subharmonic, turbulent, intermittent, and back to steady again, similar to those found for changes in u_x. It is also worth observing, by comparing Figs. 5a–5c, that the dominant frequency of oscillation increases with increasing $|p_x^*|$, as would be expected on physical grounds.

A second interesting consequence of varying p_x^* is summarized in Table 1. These calculations were performed with $u_x = 0$, $Re = 10^5$, and $a_1 = 0.075$. From this table, we observe that the least-squares time-averaged Fourier decay exponent q (which is shown in Fig. 3b for a different set of conditions) changes as the type of solution changes. The value of q is somewhat analogous to the Kolmogorov exponent, but it is obtained from a time average rather than from an ensemble average. In Ref. 13, a formulation was employed for which time and ensemble averages are equivalent. We have not used such a formulation here. Nevertheless, the variation of q shown in Table 1 is significant. It shows that solutions to Burgers' equation exhibit a wide range of decay exponents with the particular value depending on p_x^* (and the various other parameter values). This is in basic agreement with results reported in Ref. 13, where it was shown that for random p_x in a certain amplitude range, a $-5/3$ exponent can be obtained from Burgers' equation. The -2 Kolmogorov exponent found in earlier work was due to the lack of any forcing other than nonzero initial conditions.

From Table 1 we see that the chaotic solution for $p_x^* = -50$ has $q = -1.73$ and a correlation coefficient of 0.95. This provides further independent verification (in addition to Fig. 3b) that our values $h = 0.009$, $K = 10$ are reasonable. We should like to have our small-scale calculations correspond to a bridging of at least the inertial and

Table 3 Flow type as a function of u_x and a_1 ($p_x^* = -42.5$, $Re = 10^5$)

u_x \ a_1	0.0	0.025	0.050	0.075	0.100	0.125
−6.25	Subharmonic	Steady	Steady	Steady	Intermittent	Steady
−3.75	Periodic	Steady	Steady	Intermittent	Turbulent	Steady
0.0	Periodic	Intermittent	Intermittent	Turbulent	Turbulent	Steady
6.25	Periodic	Subharmonic	Subharmonic	Subharmonic	Subharmonic	Steady
13.75	Periodic	Periodic	Periodic	Periodic	Periodic	Steady

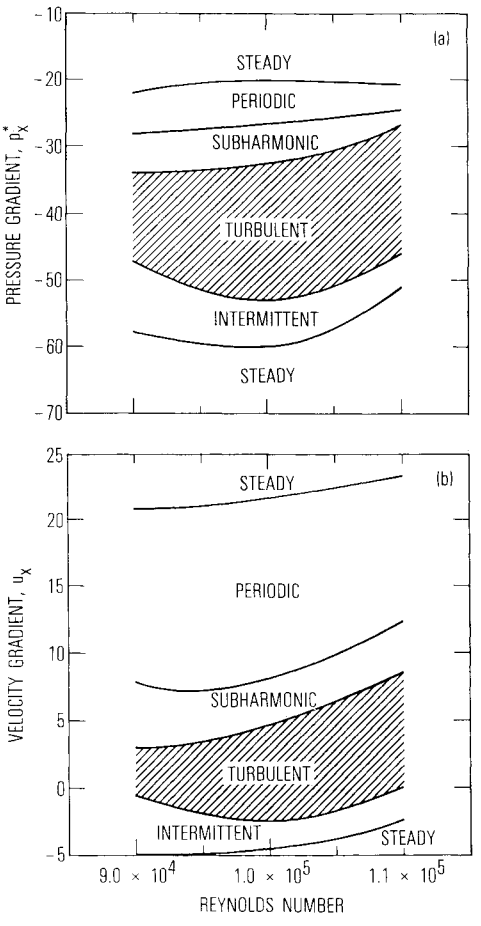

Fig. 7 Reynolds number effects: a) $u_x = 1$, b) $p_x^* = -42.5$.

dissipative ranges of a turbulent flow. Thus, the Kolmogorov exponent should be slightly smaller than $-5/3$. At the same time, the correlation coefficient must be sufficiently high to provide confidence in the actual value of the exponent. As h and K are varied, the solutions correspond to different parts of the wave-number spectrum, and the above criteria provide a method for selecting appropriate values.

The results of over 100 cases of various combinations of p_x^* and u_x, with $Re = 10^5$, $a_1 = 0.075$, are summarized in the flow regime map of Fig. 6. This map has several interesting features. First, it is clear that the basic sequence of bifurcations (steady, periodic, subharmonic, turbulent, intermittent, steady) can be achieved by varying either p_x^* or u_x over a fairly wide range of these parameters. Second, the domain of turbulent solutions is of significant size, and for most values of u_x it spans p_x^* intervals larger than the u_x intervals spanned with p_x^* fixed. This indicates stronger dependence of turbulent behavior on pressure gradient than on local flowfield velocity gradient (in the flow direction). Next, we note that two forms of steady solutions were found; these appear to meet at the dashed line. It is not presently known whether a bifurcation occurs at this line, but the steady solutions below $p_x^* \simeq -15$ and on the left side of the figure possess a much slower decay rate in time-averaged, squared Fourier coefficients than do those above this value and to the right-hand side of the figure.

A large number of computer runs were required to establish the somewhat irregular shape of the map in the upper-left corner of the figure. This is an especially interesting region because it shows that over this limited range of p_x^* and u_x, small changes in either parameter can lead to rapid flow transitions. In fact, it appears that for $u_x \simeq -15$ and $p_x^* \simeq -14.5$, a direct transition from steady to turbulent behavior may occur. Further computation is needed to assess accurately whether this actually occurs or whether a usual sequence of extremely closed spaced transitions exists.

In Fig. 7 we present partial flow regime maps that display the effects of small variations in Re about the base point $Re = 10^5$. Calculations were performed at $Re = 9 \times 10^4$ and $Re = 1.1 \times 10^5$ for $u_x = 1$, and a range of values of p_x^* (Fig. 7a) and for $p_x^* = -42.5$ for a range of values of u_x (Fig. 7b). The most important feature of these results is that they exhibit good agreement with what one intuitively expects for real turbulent flows; namely, as Re is increased, the size of the turbulent region of the regime map increases, and vice versa. Moreover, in the case of p_x^* variations, the transition to turbulence occurs more rapidly with increasing Re, as indicated by the narrowing of the periodic, subharmonic, and intermittent regions in Fig. 7a.

Our final set of results, for variation of the first small-scale Fourier coefficient a_1 is presented in Tables 2 and 3. Table 2 shows that the behavior of solutions is somewhat symmetric with respect to $a_1 = 0$, where the flow is periodic. For relatively large absolute a_1 only steady solutions are obtained, even though the other parameter values $p_x^* = -42.5$, $u_x = 1$, $Re = 10^5$ correspond to a point well inside the turbulent region shown in Fig. 6. This is believed to be due to the fact that large values of a_1 represent large-scale solutions that are not sufficiently converged to be consistently linked to small-scale solutions computed with $h = 0.009$, $K = 10$. The consequence is a steady state on the small scale that is dominated by a_1. As a_1 is decreased in magnitude, the expected turbulent behavior appears; then transitions to intermittent, and finally periodic, flow occur as a_1 is decreased to zero. The precise nature of these transitions is not fully understood at present and is the subject of ongoing investigations.

Further evidence of numerous transitions is shown in Table 3. Again, $p_x^* = -42.5$, $Re = 10^5$ have been used, but now a_1 is restricted to positive values while u_x is varied. It is evident that $a_1 = 0.125$ is too large to consistently drive the small-scale calculations since steady solutions always result, independent of the location of the point on the regime map corresponding to other parameter values. On the other hand, for $a_1 \leq 0.1$, various interesting transitions occur as a_1 is changed, especially for smaller values of u_x.

Summary and Conclusions

In this paper, we have presented the results of a fairly extensive parametric study of the effects of large-scale parameters on the nature of solutions to the small-scale Burgers' equation. We have provided easily applied methods for testing the convergence of grid functions corresponding to the chaotic solutions of a strange attractor, and for pro-

ducing consistent (if not strongly convergent) models by which a rich variety of flow types can be calculated from the small-scale Burgers' equation. The results show that these flows (and their associated transitions) are surprisingly similar to those observed in nature, corresponding to the Navier-Stokes equations. Because of this, it is believed that the large-scale/small-scale formalism currently being applied to Burgers' equation will provide a means of computing details of turbulent solutions to the Navier-Stokes equations as well. This is particularly evident from the fact that locally one-dimensional (LOD) time splittings (cf. Mitchell and Griffiths[25]) of the Navier-Stokes equations result in equations formally equivalent to a forced Burgers' equation at each split step.

From the above results and discussions, we derive the following conclusions. First, the small-scale Burgers' equation exhibits a rich variety of flow types and bifurcation sequences as the large-scale parameters are varied; the bifurcation sequences are of a basically Ruelle-Takens type, but with either Feigenbaum period doubling or Pomeau-Manneville intermittency usually replacing the quasiperiodic state. Second, each of the large-scale parameters has an associated bifurcation sequence although, clearly, these sequences are all similar. Third, it has been demonstrated, in agreement with the work of Qian, that Burgers' equation can exhibit other than a value of -2 for the Kolmogorov exponent. In fact, a wide range of squared Fourier coefficient decay exponents have been found in the present study of the small-scale equations as the large-scale parameters are varied. Finally, we have shown that there are straightforward and consistent ways to verify numerical and functional analytic approximations of chaotic solutions associated with a strange attractor, and we have employed these techniques to produce the results presented herein. This is a crucial step in applying the theory of strange attractors to the generation of subgrid scale models both for large eddy simulation and, more particularly, in the context of the large-scale/small-scale decomposition formalism.

References

[1]Ruelle, D. and Takens, F., "On the Nature of Turbulence," *Communications in Mathematical Physics,* Vol. 20, 1971, pp. 167-192.

[2]Landau, L.D. and Lifshitz, E.M., *Fluid Mechanics,* Pergamon Press, Oxford, England, 1959.

[3]Gollub, J.P. and Benson, S.V., "Many Routes to Turbulent Convection," *Journal of Fluid Mechanics,* Vol. 100, 1980, pp. 449-470.

[4]Pomeau, Y., "The Intermittent Transition to Turbulence," *Nonlinear Dynamics and Turbulence,* edited by G.I. Barenblatt, G. Iooss, and D.D. Joseph, Pitman Publishing, London, 1983.

[5]Feigenbaum, M.J., "The Transition to Aperiodic Behavior in Turbulent Systems," *Communications in Mathematical Physics,* Vol. 77, 1980, pp. 65-86.

[6]Hussain, A.K.M.F., "Coherent Structures—Reality and Myth," *Physics of Fluids,* Vol. 26, 1983, pp. 2816-2850.

[7]Rogallo, R.S. and Moin, P., "Numerical Simulation of Turbulent Flows," *Annual Review of Fluid Mechanics,* Vol. 16, 1984, pp. 99-137.

[8]Deissler, R.G., "Turbulent Solutions of the Equations of Fluid Motion," *Reviews of Modern Physics,* Vol. 56, 1984, pp. 223-254.

[9]Grötzbach, G., "Direct Numerical Simulation of Laminar and Turbulent Bénard Convection," *Journal of Fluid Mechanics,* Vol. 119, 1982, pp. 27-53.

[10]Feiereisen, W.J., Shirani, E., Ferziger, J.H., and Reynolds, W.C., "Direct Simulation of Homogeneous Turbulent Shear Flows on the Illiac IV Computer: Application to Compressible and Incompressible Modelling," *Turbulent Shear Flows 3,* edited by L.J.S. Bradbury et al., Springer-Verlag, Berlin, 1982, pp. 309-319.

[11]McDonough, J.M., Bywater, R.J., and Buell, J.C., "An Investigation of Strange Attractor Theory and Small-Scale Turbulence," AIAA Paper 84-1674, June 1984.

[12]McDonough, J.M., Buell, J.C., and Bywater, R.J., "A Comparison of Routes to a Strange Attractor in One-Dimensional Local Models of Turbulent Free and Forced Convection," ASME Paper 84-WA/HT-16, Dec. 1984.

[13]Qian, J., "Numerical Experiments on One-Dimensional Model of Turbulence," *Physics of Fluids,* Vol. 27, 1984, pp. 1957-1965.

[14]Kantorovich, L.V. and Akilov, G.P., *Functional Analysis,* 2nd ed., Pergamon Press, Oxford, England, 1982.

[15]Yakhot, V. and Orszag, S.A., "Renormalization Group Formulation of Large Eddy Simulation," *Nonlinear Dynamics of Transcritical Flows*, edited by H.L. Jordan, H. Oertel, and K. Roberts, *Lecture Notes in Engineering 13*, Springer-Verlag, Berlin, 1985, pp. 155-174.

[16]Huang, M.T. and McDonough, J.M., "Numerical Analysis of Strange Attractors—The Lorenz Equations," presented at 37th Meeting of Division of Fluid Dynamics, American Physical Society, Providence, RI, Nov. 1984; to be submitted to *Journal of Computational Physics,* 1986.

[17]Gear, C.W., *Numerical Initial Value Problems in Ordinary Differential Equations,* Prentice-Hall, Englewood Cliffs, NJ, 1971.

[18]Franceschini, V., "Two Models of Truncated Navier-Stokes Equations on a Two-Dimensional Torus," *Physics of Fluids,* Vol. 26, 1983, pp. 433-447.

[19]Treve, Y.M., "Energy-Conserving Galerkin Approximations for the Bénard Problem," *Nonlinear Dynamics and Turbulence,* edited by G.I. Barenblatt, G. Iooss, and D.D. Joseph, Pitman Publishing, London, 1983 pp. 334-342.

[20]McDonough, J.M. and Bywater, R.J., "Convergence of Fourier-Galerkin Approximations to Chaotic Solutions of Burgers' Equation," presented at 37th Meeting of Division of Fluid Dynamics, American Physical Society, Providence, RI, Nov. 1984.

[21]Constantin, P., Foias, C., Manley, O.P., and Temam, R., "Determining Modes and Fractal Dimension of Turbulent Flows," *Journal of Fluid Mechanics,* Vol. 150, 1985, pp. 427-440.

[22]Lorenz, E.N., "Deterministic Nonperiodic Flow," *Journal of Atmospheric Sciences,* Vol. 20, 1963, pp. 130-141.

[23]Creveling, H.F., de Paz, J.F., Baladi, J.Y., and Schoenhals, R.J., "Stability Characteristics of a Single-Phase Free Convection Loop," *Journal of Fluid Mechanics,* Vol. 67, 1975, pp. 65-84.

[24]Otnes, R.K. and Enochson, L., *Digital Time Series Analysis,* John Wiley & Sons, New York, 1972.

[25]Mitchell, A.R. and Griffiths, D.F., *The Finite Difference Method in Partial Differential Equations,* John Wiley & Sons, New York, 1980.